How to cite: *Angew. Chem. Int. Ed.* **2026**, *65*, e22461
doi.org/10.1002/anie.202522461

Photo-Assisted Zinc-Ion Batteries

Photoinduced Proton-Cation Cascade Boosting Ion Intercalation Dynamics in Photo-Assisted Zinc-Ion Batteries

Wenwen Zha[+], Qiushi Ruan[+], Mengyun Yang, Jiaqiang Huang, Litao Sun, ZhengMing Sun,* and Li Tao**

Abstract: While photo-assisted ion batteries represent a promising energy storage frontier—with light irradiation significantly improving performance—their development remains hindered by a fundamental knowledge gap, as existing theories struggle to fully account for improved light-driven ion intercalation. This work discovers the photoinduced proton-zinc ion intercalation cascade mechanism, establishing a theoretical framework that explains the synergistic proton-cation interplay and its role in capacity enhancement under illumination. Through light-induced charge transfer, photogenerated electrons drive proton intercalation, which induces the deprotonation of Zn^{2+}-coordinated water molecules due to the limited availability of free protons in the electrolyte. This deprotonation is energetically favored because of the lower deprotonation barrier of Zn^{2+}-coordinated water compared to uncoordinated water, thereby accelerating zinc-ion desolvation and promoting Zn^{2+} intercalation. Consequently, the synergistic H^+/Zn^{2+} co-intercalation enables an exceptional areal capacity of 12.86 mA h cm^{-2} under illumination in a photo-assisted zinc-ion battery with a high mass-loading of 30 mg cm^{-2}. This work elucidates a proton-cation cascade mechanism that governs light-driven intercalation dynamics, providing the missing link between photo-excitation and enhanced battery performance.

Introduction

Advanced renewable energy storage technologies are critical for addressing global climate challenges and achieving carbon neutrality[1,2] Photo-assisted energy storage systems, which couple optical fields and electrochemical processes, offer a promising approach to significantly enhance battery performance.[3–5] Devices integrating photovoltaic technology and energy storage have emerged as promising solutions, including photo-assisted lithium-ion batteries,[6] lithium-sulfur batteries,[7] zinc-air batteries,[8] zinc-ion batteries,[9,10] and Zn-CO_2 batteries.[11] Under illumination, these systems use semiconductor photoelectrodes to generate photoexcited charge carriers, significantly enhancing battery performance by accelerating electrode kinetics, raising voltage platforms, and boosting energy density.[12,13]

In 2020, Michael De Volder and colleagues first reported a photo-assisted zinc-ion battery utilizing V_2O_5 as a dual-functional active material capable of capturing visible light while storing ions, boosting capacity from 190 to 370 mA h g^{-1} at 50 mA g^{-1} under illumination.[14] Subsequently, researchers employing materials such as V_2O_5,[6] VO_2,[15] and others have demonstrated light-charging capabilities with solar-to-energy conversion efficiencies reaching 1.8%.[6] Our group expanded this field by elucidating the critical role of photo-induced proton transport in enhancing capacity and stability (90% capacity retention after 4000 cycles),[16] and demonstrating the "irradiation spillover effect," which is promising to resolve illumination area constraints in highly integrated photo-assisted zinc-ion battery systems.[9] Despite these breakthroughs, a fundamental mechanistic gap persists, as current theory cannot fully describe light-driven ion intercalation dynamics.

While successfully ascribing photo-charging behavior to band-structure-mediated carrier transfer to the zinc anode, photovoltaic theory cannot explain the dramatic enhancements in discharge capacity and ion intercalation kinetics observed under illumination.[17–19] Attributing these solely to the high energy of photogenerated electrons also neglects the intricacies of light-driven ion intercalation.[14,20,21] Although photo-induced proton transport partially explains enhanced ion intercalation kinetics,[9,16] at higher mass loading electrodes, the scarcity of free protons compared to the active material constrains the applicability of the photoinduced proton transport mechanism. To date, the better-than-expected performance of photo-assisted zinc-ion battery challenges the validity of the existing theories models, and the ambiguous charge transfer mechanisms hinder the development of advanced photo-assisted ion batteries.[17]

Herein, we propose a newly discovered cascade mechanism in which light-induced proton intercalation facilitates

[*] W. Zha[+], Q. Ruan[+], M. Yang, J. Huang, Z. Sun, L. Tao
School of Materials Science and Engineering, Southeast University, Nanjing 211189, P.R. China
E-mail: ruanqs@seu.edu.cn
zmsun@seu.edu.cn
tao@seu.edu.cn

L. Sun, L. Tao
SEU-FEI Nano-Pico Center, Key Laboratory of MEMS of Ministry of Education, Southeast University, Nanjing 210096, P.R. China

[+] Both authors contributed equally to this work.

Additional supporting information can be found online in the Supporting Information section

subsequent Zn^{2+} intercalation through a deprotonation process. Photogenerated electrons enhance proton intercalation via photoinduced proton transfer. This accelerates the deprotonation of Zn^{2+}-coordinated water molecules, significantly improving Zn^{2+} desolvation kinetics and accelerating subsequent Zn^{2+} intercalation. Both experimental and first-principles computational results confirm Zn^{2+}-coordinated water as the primary source of intercalated protons. This photoinduced proton-zinc ion cascade accelerates interfacial kinetics, significantly enhancing battery performance under illumination. At high mass loading, the limited availability of free protons relative to the active material renders the proton-zinc ion cascade mechanism more prominent than in low-mass-loading electrodes, enabling outstanding capacity and rate capability (280 mA h g^{-1} at 5 A g^{-1} with 6.75 mg cm^{-2} mass-loading). Notably, an ultrahigh areal capacity of 12.86 mA h cm^{-2} with a high mass-loading electrode (30 mg cm^{-2}) was achieved, demonstrating the commercial potential of photo-assisted zinc-ion batteries.

Results and Discussion

A basic model of photo-assisted zinc-ion battery was illustrated in Figure S1.[9,16] Mn pre-intercalated hydrated vanadium pentoxide (MnVO) was selected as the cathode material due to its robust performance in the dark and visible light absorption (the morphology and crystal structure were confirmed by SEM and XRD in Figure S2a–c, respectively; absorption spectra was shown in Figure S2d).[22] The impact of light irradiation on battery performance was evaluated using a coin-cell configuration with an optical window (the configuration is illustrated in Figure S3). Electrodes were fabricated via dry-processable electrode technology with a mass loading from 5 to 30 mg cm^{-2} (Figure S4).

Cyclic voltammetry (CV) curves under light and dark conditions were compared. As shown in Figure 1a, two redox peaks at 0.5 mV s^{-1} correspond to the valence transitions of V^{5+}/V^{4+} and V^{4+}/V^{3+}.[23] Under light illumination, significant shifts of the redox peak positions were observed, with the oxidation peaks shifting to the lower potential (ΔV_1 = -0.032 V, ΔV_2 = -0.050 V) and reduction peaks shifting to the higher potential (ΔV_3 = 0.034 V, ΔV_4 = 0.029 V) (Figure S5), the shift of the CV peak may be related to electronic structure change of MnVO material upon light (indicated by open-circuit voltage in Figure S6). This results in a marked reduction in the polarization of the redox reactions (V^{4+}/V^{3+}: 0.245 → 0.179 V, V^{5+}/V^{4+}: 0.16 → 0.081 V) (Figure 1a), which indicates higher reversibility and faster electrochemical kinetics of the battery under illumination.[23,24] Additionally, the increased integrated area and peak current densities of the CV curve under illumination suggest higher electrochemical reactivity and capacity. Galvanostatic discharge–charge (GCD) profiles further confirm that light significantly enhances both plateau potentials and capacity. At a specific current of 1 A g^{-1}, the capacity increases by ~33.3% (from 300 to 400 mA h g^{-1}) under illumination (Figure 1b). Further comparison of rate performance under light and dark conditions (Figure 1c) reveals that the promoting effect of light on capacity is more significant at high current densities compared with low current densities. For instance, at 5 A g^{-1}, the capacity increases by 50.1% under illumination (Figure S7). The smaller polarization in higher scan-rate CV curves further confirms that light accelerates interfacial reaction kinetics (Figure S5).[24] The observed capacity enhancement is primarily attributed to the absorption of high-energy photons (λ < 550 nm) by MnVO (details are displayed in Figures S2d and S8).

To elucidate the mechanism by which light affects the electrochemical behavior of batteries, the pseudocapacitance behavior and ion diffusion were investigated in illuminated and dark conditions. As shown in Figure S9, the b values were calculated through CV curves obtained under different scan rates in illuminated and dark conditions, the b values between 0.5–1 indicating co-control of the electrochemical reaction by ion diffusion and pseudocapacitance behavior.[25] From the fitting results, it can be seen that compared to the dark condition (b values of peaks 1, 2, 3, and 4 were 0.524, 0.740, 0.697, and 0.706, respectively), the b values under illumination were significantly increased (b values of peaks 1, 2, 3, and 4 were 0.728, 0.872, 0.796, and 0.801, respectively),[16] suggesting promoted pseudocapacitive behavior. For instance, at 0.4 mV s^{-1} scan rate, the pseudocapacitance contribution increases from 62% to 68% under illumination (Figures 1d and S10 and S11). The fast interfacial redox kinetics represented by pseudocapacitance behavior may be key to the superior rate performance under illumination.[15,26] Impedance analysis (Figures 1e and S12, and Table S1) reveals that illumination significantly reduces interfacial charge transfer resistance (2.652→1.787 Ω). Reduced battery polarization further confirms the effect of light on promoting interfacial reaction kinetics (Figure 1f).[27] The activation polarization (η_{ac}) decreases from 20.7 mV to 7.1 mV (with negligible change in ohmic polarization (η_{ohm}), Table S1), indicating a lowered reaction energy barrier and accelerated charge transfer at the interface. Concurrently, concentration polarization (η_{con}) decreases from 90.8 to 45.8 mV, reflecting that reactant concentration differences were reduced between the electrode surface and bulk electrolyte. This suggests enhanced proton/zinc ion transfer kinetics to the electrode surface, potentially attributed to photo-induced electric fields.[28] The Galvanostatic Intermittent Titration Technique results (Figures 1g and S13) demonstrate that illumination also facilitates ion diffusion, but not significant.[16] Furthermore, an infrared (IR) cut experiment was performed to isolate the photothermal effect on capacity contributions. As a result, the thermal effect brought by infrared light contributes only 17.7% to the capacity enhancement (Figure S14), demonstrating that photon-driven processes dominate the capacity improvement.

In conclusion, the exceptional rate performance under illumination can be attributed to significantly improved interfacial kinetics, encompassing both accelerated charge transfer and enhanced ion diffusion. Consequently, the energy density and power density of dry-processable zinc-ion battery electrodes (6.75 mg cm^{-2}) are substantially improved under illumination. Notably, the energy density increases by 51.4% at high power density (Dark: 113.57 Wh kg^{-1} at 3194.65 W

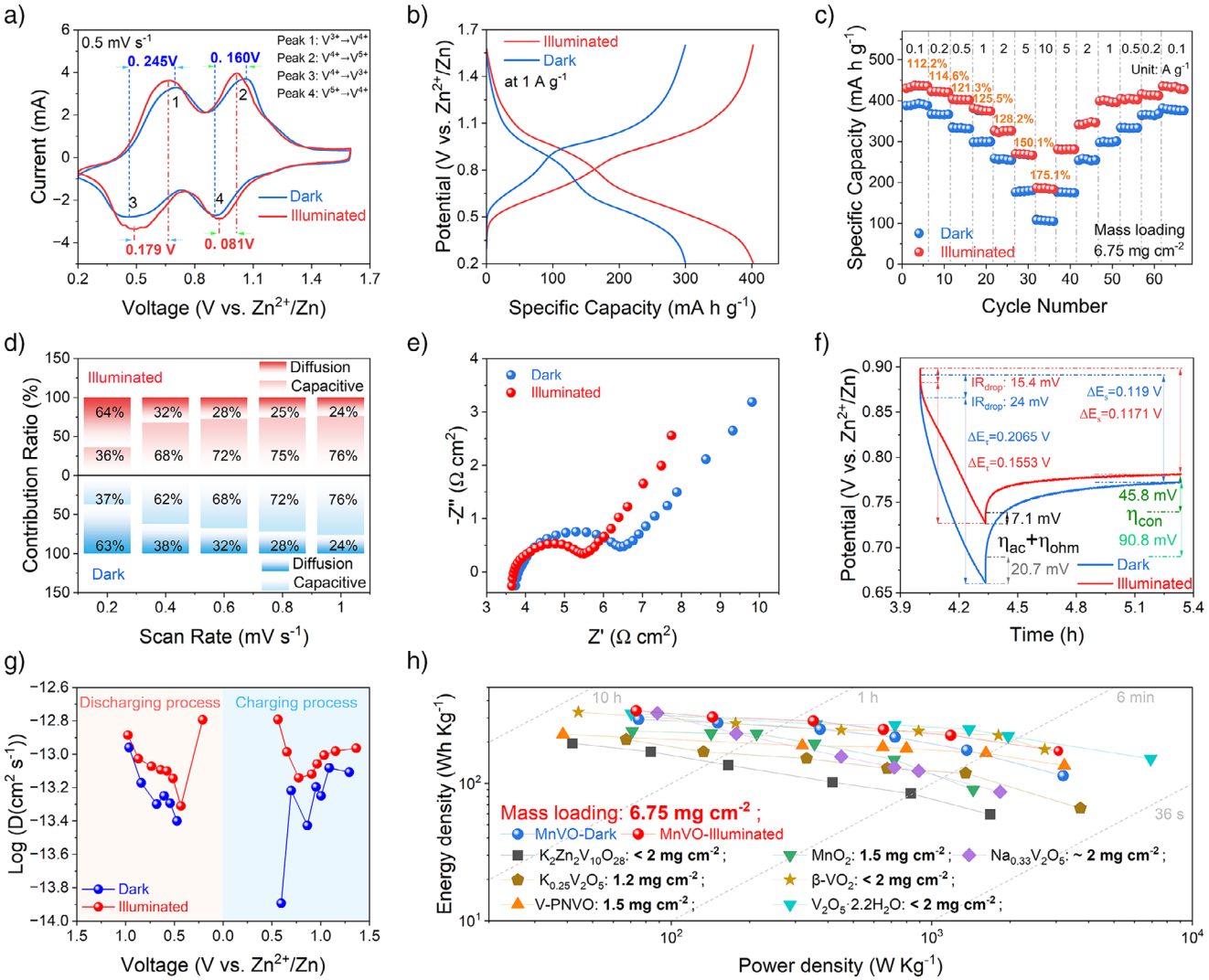

Figure 1. The promoting effect of light on zinc-ion battery performance. a) Cyclic voltammetry curves at 0.5 mV s^{-1} in dark and illuminated conditions. b) Galvanostatic charge-discharge profiles at 1 A g^{-1} in dark and illuminated conditions. c) Rate performance at 0.1–10 A g^{-1} of MnVO-based zinc-ion battery in dark and illuminated conditions. d) The capacitive contributions at different scan rates in dark and illuminated conditions. e) EIS plots of the MnVO cathode in dark and illuminated conditions. f) The kinetic polarization decoupling analysis regarding the galvanostatic intermittent titration technique (η_{ac}: activation polarization; η_{con}: concentration polarization; η_{ohm}: ohmic polarization). g) Evaluated diffusion coefficients of ions in dark and illuminated conditions. h) Energy density comparison between the high mass-loading MnVO cathode (6.75 mg cm^{-2}) and reported cathodes with low mass loading (< 2 mg cm^{-2}).

kg^{-1}; Illumination: 172 Wh kg^{-1} at 3062.9 W kg^{-1}), even outperforming other reported aqueous zinc-ion batteries with low mass-loading (e.g., 338 Wh kg^{-1} at 73.4 W kg^{-1}) (Figure 1h),[25,29–35] achieving both high energy density and power density.

To further investigate the mechanism of light-accelerated interfacial reaction kinetics, time-of-flight secondary ion mass spectrometry (TOF-SIMS) was used to analyze ion intercalation behavior in full-discharged electrodes under illuminated and dark conditions, and the H and Zn signals were normalized by using vanadium oxide as a reference. Light enhances discharge capacity more prominently (19.7%) than charge capacity (7.96%) (Figure S15), suggesting that photo-generated electrons facilitate ion intercalation more effectively than photo-generated holes facilitate ion deintercalation, likely due to the larger effective mass of holes. Therefore, we focus on the light-driven ion intercalation process here. The TOF-SIMS results demonstrate that the signal intensity of proton and zinc ions is increased significantly under illumination, which suggests that more protons and zinc-ions intercalate into the electrode (Figure 2a,b). Notably, light exhibits pronounced promotion effects on proton intercalation, which is identified as the key factor enabling superior rate performance due to the rapid reaction kinetics of protons.[16] However, the specific process underlying photo-enhanced zinc ion intercalation remains unclear.

To clarify the mechanism of light in promoting zinc-ion intercalation, comparative analysis of capacity contributions at different potentials under illuminated and dark conditions

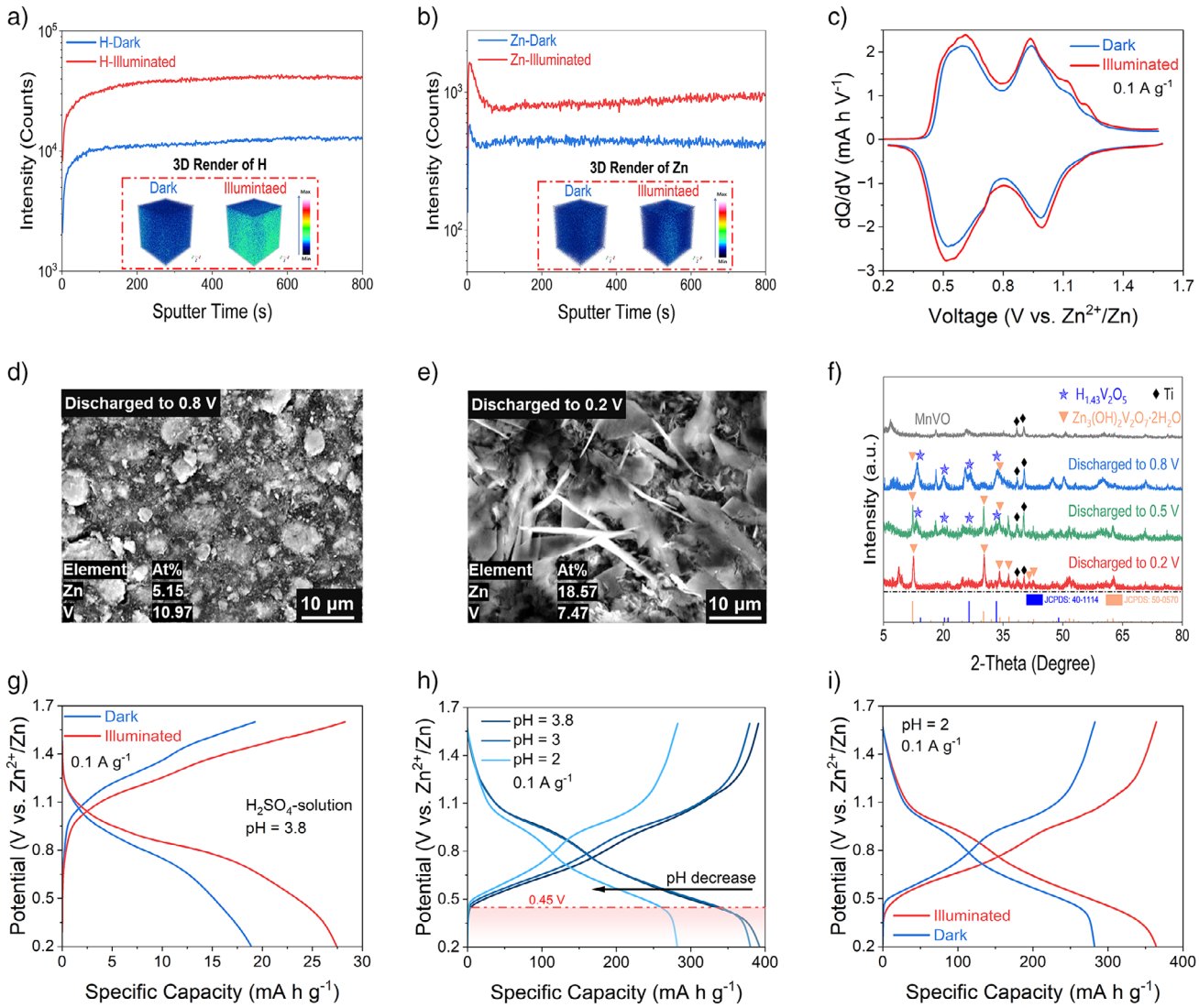

Figure 2. The origin of promoting performance in high mass-loading electrodes by illuminating; a) The TOF-SIMS depth profile and the reconstructed 3D spatial fragment distributions (insert) of H. b) The TOF-SIMS depth profile and the reconstructed 3D spatial fragment distributions (insert) of Zn. c) The differential capacity (dQ/dV) curves of GCD at 0.1 A g^{-1} in dark and illuminated conditions (PH = 2). d) Electrodes discharged to 0.8 V in illuminated conditions, SEM images. e) Electrodes discharged to 0.2 V in illuminated conditions, SEM images. f) Pristine electrodes and electrodes discharged to 0.8, 0.5, and 0.2 V in illuminated conditions, ex situ XRD patterns. g) GCD profiles at a specific current of 0.1 A g^{-1} in dark and illuminated conditions (H_2SO_4 solution, PH = 3.8). h) GCD profiles at a specific current of 0.1 A g^{-1} in dark conditions (Add H_2SO_4 and adjust PH to 3.8, 3, 2). i) GCD profiles at a specific current of 0.1 A g^{-1} in dark and illuminated conditions (PH = 2).

revealed two characteristic peaks in the differential capacity (dQ/dV) curves of Galvanostatic charge–discharge profiles, located near 1 and 0.5 V, respectively, representing the main reaction plateau potentials contributing to capacity. Notably, light significantly enhanced the capacity contribution near 0.5 V (Figure 2c). To elucidate the battery reactions corresponding to these two peaks, XRD and SEM analyses were performed on electrodes discharged to 0.8 and 0.2 V. The electrode discharged to 0.8 V showed no significant surface morphology changes (Figures 2d and S16), while XRD revealed the emergence of a new $H_{1.43}V_2O_5$ phase with a little $Zn_3(OH)_2V_2O_7{\cdot}2H_2O$ (ZVO) phase (Figure 2f), and the electrode discharged to 0.5 and 0.2 V exhibited abundant lamellar ZVO phases (Figures 2e,f, and S17). This is due to the interfacial alkaline environment caused by the intercalation of a large number of protons, which induces the growth of alkaline byproducts (ZVO phase),[36] indicating proton intercalation persisted throughout the overall discharge process.[25]

H_2SO_4 electrolytes with a pH of 3.8 were used to clarify the source of intercalation proton. Without Zn^{2+}, proton intercalation provides limited capacity in high mass-loading electrodes, unlike in low mass-loading ones where free-proton intercalation dominates (Figures 2g and S18).[37] This suggests that free proton is not the main intercalation proton source of boosted capacity in high-mass loading electrodes, and the significant increase in capacity under illumination is closely related to the intercalation of zinc ions. Increasing free H^+

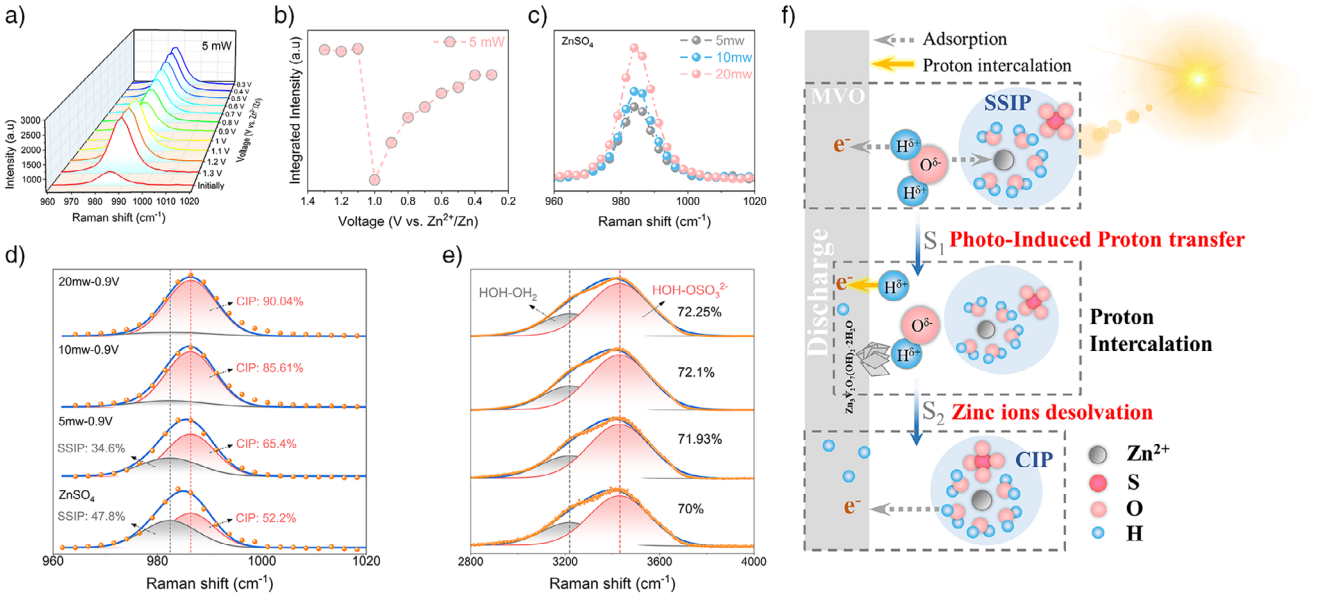

Figure 3. The evidence of light promoted desolvation of zinc ions. a) In situ Raman spectra of the ν-SO_4^{2-} bond. b) concentration (Raman peak Integral intensity) of the ν-SO_4^{2-} bond at different Voltage (5 mW). c) In situ Raman spectra of the ν-SO_4^{2-} bond for $ZnSO_4$ electrolytes at different light intensities (without any bias). d) In situ Raman spectra of the ν-SO_4^{2-} bond and e) the O—H stretch vibration for $ZnSO_4$ electrolytes at different light intensity (0.9 V). f) Schematic diagram of photo-induced proton intercalation promoting the desolvation process of the zinc ion.

concentration of electrolyte from pH∼3.8 to pH∼2 by adding H_2SO_4 causes a capacity decrease from 391 to 282 mA h g^{-1} (Figure 2H), suggesting that the zinc ion intercalation behavior is suppressed by the high concentration of free H^+.[25] In an acidified electrolyte (pH∼2), the capacity increased from 282 to 364.5 mA h g^{-1} upon illumination, similar to the dark capacity in an electrolyte with a lower H^+ concentration (pH∼3) (Figure 2i). It indicated a cascade effect that photo-induced proton intercalation facilitates zinc ion intercalation. Since free H^+ has a limited capacity contribution and unfavorable effect in such system (Figure 2g,h), it can be speculated that light-driven intercalated protons primarily originate from Zn^{2+}-coordinated water, thereby accelerating the desolvation of zinc ions and promoting zinc ion intercalation.

To further verify the promoting effect of photo-induced proton intercalation on the zinc ion desolvation kinetics, in situ Raman spectroscopy was employed to monitor the desolvation behavior of zinc ions at the electrode surface during the discharging process in real time (Figure S19). In typical 2 M $ZnSO_4$ solutions, Zn^{2+} exists as a hexahydrate, namely, solvent separated ion pair (SSIP, $[Zn^{2+}(H_2O)_6{\cdot}SO_4^{2-}]$) in the outer-sphere solvation structure. Boosting the $ZnSO_4$ concentration would strengthen the ion-pair into a contact ion pair (CIP, $[Zn^{2+}(H_2O)_5{\cdot}SO_4^{2-}]$) in the inner-sphere by loss of one water of hydration.[38] From the in situ Raman spectra, it can be observed that the peak position and intensity at ∼986 cm^{-1} exhibit significant changes as the voltage decreases (Figures 3a and S20). This peak is typically assigned to ν-SO_4^{2-} (SSIP and CIP) and can be used to determine the change in zinc-ion concentration.[39] Compared with the original peak, the peak intensity significantly increases when discharged. This is due to the gradual migration of ions towards the electrode surface under the influence of the electric field, leading to an increase in zinc ion (CIP/SSIP) concentration at the interface.[40] Discharging to 1 V, a significant decrease in the peak of ν-SO_4^{2-} integration intensity indicates an intense proton intercalation into the electrode[40] (Figure 3b), suggesting a rapid decrease in CIP/SSIP concentration at the interface caused by intercalated protons from Zn^{2+}-coordinated water. However, as the reaction proceeds further, the peak integration intensity gradually increases with the decrease in voltage, suggesting a slowdown in the rate of ion intercalation kinetics at the interface.

Simultaneously, the influence of light intensity on electrochemical reactions was investigated by modulating illumination power. It was observed that under open-circuit conditions (without applied voltage), increasing light intensity only amplified the Raman peak intensity at 984 cm^{-1} without peak shift (Figure 3c), which means that light will not affect the solvation structure of zinc ions without interface electrochemical reaction. Raman spectra of $ZnSO_4$ electrolytes with different concentrations show that higher concentrations induced a pronounced red shift of the Raman peak (∼984 cm^{-1}), which indicates the higher CIP proportion (Figure S21).[41] Further analysis of the effects of light (Figure 3d) during the discharging process reveals a distinct redshift in the ν-SO_4^{2-} peak with increasing light intensity. The ν-SO_4^{2-} bond, centered at 982–986 cm^{-1}, can be assigned to two main species, i.e., solvent-shared ion pair (SSIP ∼982 cm^{-1}) and contact ion pair (CIP ∼986 cm^{-1}).[41] Fitting of in situ Raman spectra at 0.9 V under varying light intensity shows a significant increase in CIP proportion (65.4% → 90.04%) accompanied by SSIP reduction with increasing light intensity, indicating light-induced conversion from SSIP to CIP species. This transformation suggests accelerated Zn^{2+}

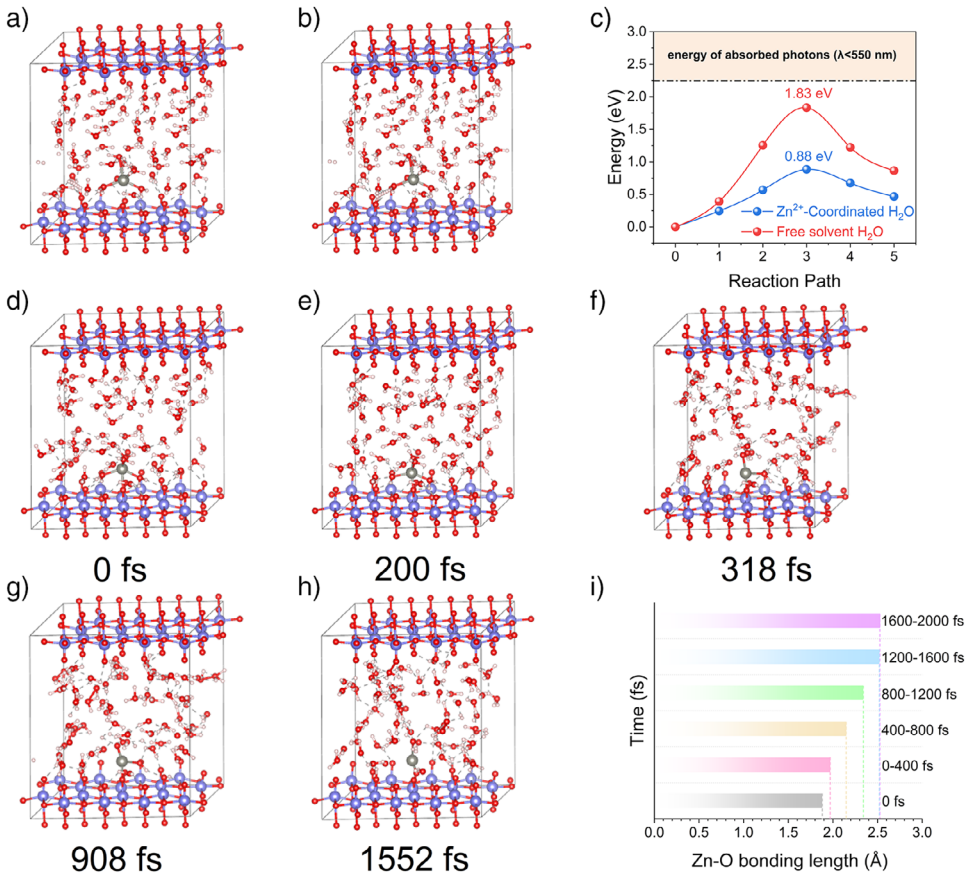

Figure 4. First principles calculations and molecular dynamics simulations. First principles calculations: deprotonation process of a) free solvent water and b) Zn^{2+}-coordinated water c) activation energy of deprotonation reaction of free solvent water and Zn^{2+}-coordinated water, compared with the energy of absorbed photons. Molecular dynamics simulations: snapshots of the typical desolvation process of zinc ions at different times d) 0 fs. e) 200 fs. f) 318 fs. g) 908 fs. h) 1552 fs. i) The average bond length of the Zn—O bond at different times (O is from Zn^{2+}-coordinated water). (Red sphere: O; Pink sphere: H; Blue sphere: V; Grey sphere: Zn).

ion desolvation under illumination. The preserved hydrogen-bonding network (Figures 3e and S22) further confirms that Zn^{2+}-coordinated water can be deprotonated in the presence of free electrolyte water.[38] The pronounced enhancement of the zinc-ions desolvation process under illumination is accelerated by photo-induced proton intercalation, driving SSIP species dehydration and rapid conversion to CIP species (Figure 3f).

In situ Raman evidence concludes that the improvement of interfacial reaction kinetics by illumination is fundamentally due to the acceleration of the desolvation process of zinc ions by Zn^{2+}-coordinated water deprotonation through photo-induced proton intercalation. The synchronous improvement of proton/zinc ion intercalation kinetics under illumination is crucial for achieving good performance in photo-assisted batteries.

First-principles calculations further confirm that the Zn^{2+}-coordinated water is more prone to dissociate into H^+ and OH^- compared to free solvent water (Figure 4a,b). The deprotonation reaction barriers for Zn^{2+}-coordinated water and free solvent water were calculated separately, revealing that the barrier for Zn^{2+}-coordinated water (0.88 eV) is lower than that for free solvent water (1.83 eV) (Figure 4c). This difference arises because free solvent water lacks the local electronic polarization induced by Zn^{2+} coordination, which weakens the O—H bond. Since photons with wavelengths shorter than 550 nm (energies above 2.25 eV) are absorbed by the material (Figure S2D), they provide sufficient energy to overcome the dissociation barrier of Zn^{2+}-coordinated water. Although the photon energy also exceeds the barrier for free water, the absence of such polarization results in a smaller effective driving force, making deprotonation of free water less efficient under illumination.

To further understand the zinc-ion desolvation process at the atomic scale, molecular dynamics simulations were employed to study the changes in the solvation structures around zinc ions during the discharge process. Several snapshots were selected within a timescale of 1552 femtoseconds (fs). It can be observed that when the hydrated zinc ion adsorbs onto the MnVO surface (at 0 fs) (Figure 4d), the negatively charged hydroxyl groups at the interface attract the hydrogen atoms of Zn^{2+}-coordinated water molecules, leading to the formation of chemical bonds and subsequent deprotonation of the Zn^{2+}-coordinated water molecules (at 200 fs) (Figure 4e). As the reaction progresses, the Zn^{2+}-coordinated water is gradually stripped away (from 318 to 1552 fs), accompanied by the breaking of coordination bonds (Figure 4f–h). The average Zn—O bond length increases from

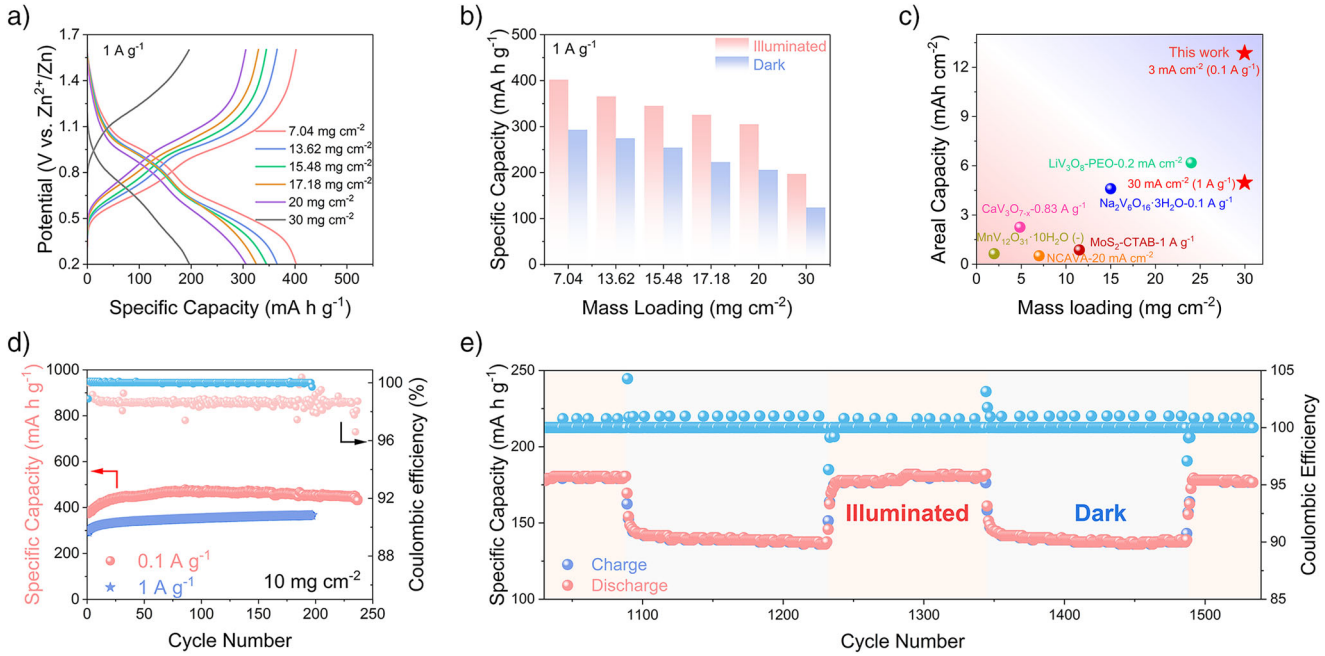

Figure 5. Performance on high mass-loading MnVO cathodes under illumination. a) and b) Capacity of electrodes with different mass loading in illuminated and dark conditions at a current density of 1 A g^{-1}. c) Comparison of the MnVO cathode with the reported high mass-loading cathodes for AZIBs. d) Long-term cycling performance at a specific current of 0.1 and 1 A g^{-1} in dark conditions (10 mg cm^{-2}). e) GCD cycling at a specific current of 5 A g^{-1} in dark/illuminated conditions (10 mg cm^{-2}). [Correction added on November 9, 2025, after first online publication: Figure 5c has been updated.]

1.88 to 2.53 Å (Figure 4i). Therefore, light-driven intercalated protons primarily originate from Zn^{2+}-coordinated water molecules, promoting the desolvation of zinc ions and thus enhancing the zinc ion intercalation kinetics via a cascade effect.

The proton-zinc ion cascade mechanism is expected to be more prominent at high mass-loading conditions as the availability of free protons relative to the active material becomes limited (Figure S18). To verify the feasibility of photo-assisted cells with high mass loading, a series of electrodes with high loadings (5-30 mg cm^{-2}) was tested. Although light penetration into the electrode is limited relative to its thickness (Figure S23), the migration of photogenerated electrons allows deeper regions to be affected, thereby enhancing the performance of high mass-loading electrodes.[9] Under illumination at a high current density of 1 A g^{-1}, the electrode maintained excellent performance even with high mass loadings of 20 and 30 mg cm^{-2}, delivering specific capacities of 305.04 and 197 mA h g^{-1}, respectively (Figure 5a). Notably, illumination enhanced the battery's specific capacity by 48% and 60% compared to dark conditions for these loadings (Figures 5B and S24). The excellent performance further confirms the significant role of light in promoting proton/zinc ion intercalation, which enables photo-assisted batteries exhibiting impressive areal capacities (12.86 mA h cm^{-2} at 3 mA cm^{-2}, 4.97 mA h cm^{-2} at 30 mA cm^{-2}), which is higher than previously reported capacity performance for high mass-loading electrode (Figures 5c and S25).[35,42–46]

By employing an alloying strategy (zinc-indium alloy interface modification), dendrite growth and hydrogen evolution corrosion were suppressed (Figures S26 and S27).[47] At current densities of 0.1 and 1 A g^{-1}, the electrodes demonstrated stable operation over 2000 h and 200 cycles (Figure 5d). The XPS and XRD results both showed that the MnVO phase was well preserved after cycling (Figure S28), and the side reaction, e.g., the hydrogen evolution reaction, is responsible for a CE slightly lower than 100%. Under light-dark cycling, batteries operating at a high current density of 5 A g^{-1} could maintain stability for more than 1500 cycles (Figure 5e). The excellent stability and rate performance demonstrate the great potential of photo-assisted zinc-ion batteries in practical applications (Table S2).

Conclusion

In summary, this work reveals the photoinduced proton-cation intercalation cascade mechanism, where photogenerated electrons first deplete free protons on the surface via intercalation, triggering the deprotonation of Zn^{2+}-solvation water (energetically favored over free solvent water) to accelerate Zn^{2+} desolvation and subsequent intercalation. The synergistic intercalation of protons-zinc ions enabled an exceptional areal capacity of 12.86 mA h cm^{-2} at a high mass loading (~30 mg cm^{-2}). By uncovering a photoinduced proton-cation cascade, this study bridges a critical knowledge gap in photo-assisted ion battery systems and fundamentally explains how illumination enhances battery performance beyond existing theories.

Acknowledgements

The authors acknowledge the use and support of the School of Materials Science and Engineering, Southeast University Facilities.

Conflict of Interests

The authors declare no conflict of interest.

Data Availability Statement

The data that support the findings of this study are available from the corresponding author upon reasonable request.

Keywords: High mass-loading · Ion intercalation · Photochemistry · Solvation effects · Zinc-ion battery

[1] C. Li, S. Jin, L. A. Archer, L. F. Nazar, *Joule* **2022**, *6*, 1733–1738, https://doi.org/10.1016/j.joule.2022.06.002.
[2] G. Mahendra, R. Roy, A. K. Singh, *J. Power Sources* **2024**, *624*, 235515, https://doi.org/10.1016/j.jpowsour.2024.235515.
[3] A. Gurung, Q. Qiao, *Joule*, **2018**, *2*, 1217–1230, https://doi.org/10.1016/j.joule.2018.04.006.
[4] A. Lee, M. Vörös, W. M. Dose, J. Niklas, O. Poluektov, R. D. Schaller, H. Iddir, V. A. Maroni, E. Lee, B. Ingram, L. A. Curtiss, C. S. Johnson, *Nat. Commun.* **2019**, *10*, 4946, https://doi.org/10.1038/s41467-019-12863-6.
[5] A. Soundarya Mary, G. Mahendra, R. Roy, M. K. Ganesha, A. K. Singh, *EES Batteries*, **2025**, *1*, 23–72, https://doi.org/10.1039/D4EB00018H.
[6] B. D. Boruah, B. Wen, M. De Volder, *Nano Lett.* **2021**, *21*, 3527–3532, https://doi.org/10.1021/acs.nanolett.1c00298.
[7] Y.u-H. Liu, J. Qu, W. Chang, C.-Y.e Yang, H.-J. Liu, X.-Z. Zhai, Y.u Kang, Y.u-G. Guo, Z.-Z. Yu, *Energy Storage Mater.* **2022**, *50*, 334–343, https://doi.org/10.1016/j.ensm.2022.05.030.
[8] L. Kong, Q. Ruan, J. Qiao, P. Chen, B. Yan, W. He, W. Zhang, C. Jiang, C. Lu, Z. Sun, *Adv. Mater.* **2023**, *35*, 2304669, https://doi.org/10.1002/adma.202304669.
[9] L. Ma, Q. Ruan, W. Zha, L. Kong, Z. Sun, *Adv. Energy Mater.* **2024**, 202303586, https://doi.org/10.1002/aenm.202303586.
[10] R. Roy, G. Mahendra, A. K. Singh, *Chem. Eng. J.* **2024**, *500*, 156870, https://doi.org/10.1016/j.cej.2024.156870.
[11] X. Liu, S. Tao, J. Zhang, Y.u Zhu, R. Ma, J. Lu, *J. Mater. Chem. A*, **2021**, *9*, 26061–26068, https://doi.org/10.1039/d1ta07522e.
[12] N.-F. Yan, X.-P Gao, *Energy & Environmental Materials* **2022**, *5*, 439–451, https://doi.org/10.1002/eem2.12182.
[13] F. Chen, Y. Gao, Q. Hao, X. Chen, X. Sun, N.a Li, *ACS Nano.* **2024**, *18*, 6413–6423, https://doi.org/10.1021/acsnano.3c11851.
[14] B. D. Boruah, A. Mathieson, B.o Wen, S. Feldmann, W. M. Dose, M. De Volder, *Energy Environ. Sci.* **2020**, *13*, 2414–2421, https://doi.org/10.1039/d0ee01392g.
[15] B. Deka Boruah, A. Mathieson, S. K.i Park, X. Zhang, B.o Wen, L. Tan, A. Boies, M. De Volder, *Adv. Energy Mater.* **2021**, *11*, 2100115, https://doi.org/10.1002/aenm.202100115.
[16] W. Zha, Q. Ruan, L. Ma, M. Liu, H. Lin, L. Sun, Z. Sun, L.i Tao, *Angew. Chem. Int. Ed.*, **2024**, *63*, e202400621, https://doi.org/10.1002/anie.202400621.
[17] X. Dong, X. Chen, X. Jiang, N. Yang, *Adv. Energy Mater.* **2023**, *13*, 2301143, https://doi.org/10.1002/aenm.202301143.
[18] Y.-X. Tan, X. Zhang, J. Lin, Y. Wang, *Energy Environ. Sci.* **2023**, *16*, 2432–2447, https://doi.org/10.1039/d3ee00461a.
[19] A. Pujari, K. Shimokawa, M. De Volder, *Joule* **2025**, *9*, 101869, https://doi.org/10.1016/j.joule.2025.101869.
[20] B. D. Boruah, B. Wen, M. De Volder, *ACS Nano* **2021**, *15*, 16616–16624, https://doi.org/10.1021/acsnano.1c06372.
[21] M. Yang, D. Wang, Y. Ling, X. Guo, W. Chen, *Adv. Funct. Mater.* **2024**, *34*, https://doi.org/10.1002/adfm.202410398.
[22] J. Qian, Y. You, Z. Fan, X. Liu, J. Tang, W. He, Z. Sun, *J. Energy Storage* **2023**, *63*, 106988, https://doi.org/10.1016/j.est.2023.106988.
[23] F. Liu, Z. Chen, G. Fang, Z. Wang, Y. Cai, B. Tang, J. Zhou, S. Liang, *Nano-Micro Lett.* **2019**, *11*, 25, https://doi.org/10.1007/s40820-019-0256-2.
[24] L. Liu, T. Yuan, Z. Li, K. Chen, W. Huang, *Electrochim. Acta* **2023**, *439*, 141717, https://doi.org/10.1016/j.electacta.2022.141717.
[25] F. Wan, L. Zhang, X.i Dai, X. Wang, Z. Niu, J. Chen, *Nat. Commun.* **2018**, *9*, 1656, https://doi.org/10.1038/s41467-018-04060-8.
[26] R. Li, H. Zhang, Q. Zheng, X. Li, *J. Mater. Chem. A* **2020**, *8*, 5186–5193, https://doi.org/10.1039/c9ta11750d.
[27] Z.i-X. Chen, Q. Cheng, X.i-Y. Li, Z. Li, Y.-W. Song, F. Sun, M. Zhao, X.-Q. Zhang, B.o-Q. Li, J.-Q.i Huang, *J. Am. Chem. Soc.* **2023**, *145*, 16449–16457, https://doi.org/10.1021/jacs.3c02786.
[28] T. Defferriere, D. Klotz, J. C. Gonzalez-Rosillo, J. L. M. Rupp, H. L. Tuller, *Nat. Mater.* **2022**, *21*, 438–444, https://doi.org/10.1038/s41563-021-01181-2.
[29] H. Tang, W. Chen, N.a Li, Z. Hu, L.i Xiao, Y. Xie, L. Xi, L. Ni, Y. Zhu, *Energy Storage Mater.* **2022**, *48*, 335–343, https://doi.org/10.1016/j.ensm.2022.03.042.
[30] W. Bi, G. Gao, G. Wu, M. Atif, M.s AlSalhi, G. Cao, *Energy Storage Mater.* **2021**, *40*, 209–218, https://doi.org/10.1016/j.ensm.2021.05.003.
[31] P. He, G. Zhang, X. Liao, M. Yan, X.u Xu, Q. An, J. Liu, L. Mai, *Adv. Energy Mater.* **2018**, *8*, 1702463, https://doi.org/10.1002/aenm.201702463.
[32] S. Li, M. Chen, G. Fang, L. Shan, X. Cao, J. Huang, S. Liang, J. Zhou, *J. Alloys Compd.* **2019**, *801*, 82–89, https://doi.org/10.1016/j.jallcom.2019.06.084.
[33] T. Zhou, L. Zhu, L. Xie, Q. Han, X. Yang, X. Cao, J. Ma, *Small* **2022**, *18*, 2107102, https://doi.org/10.1002/smll.202107102.
[34] X. Fan, X. Wen, Y. Tang, W. Zhou, K. Xiang, H. Chen, *Electrochim. Acta* **2021**, *400*, 139425, https://doi.org/10.1016/j.electacta.2021.139425.
[35] M. Wu, C. Shi, J. Yang, Y. Zong, Y. Chen, Z. Ren, Y. Zhao, Z. Li, W. Zhang, L. Wang, X. Huang, W. Wen, X. Li, X. Ning, X. Ren, D. Zhu *Adv. Mater.* **2024**, *36*, e2310434-e2310434, https://doi.org/10.1002/adma.202310434.
[36] Y. Kim, Y. Park, M. Kim, J. Lee, K.i J. Kim, J. W. Choi, *Nat. Commun.* **2022**, *13*, 2371, https://doi.org/10.1038/s41467-022-29987-x.
[37] S. W. D. Gourley, R. Brown, B. D. Adams, D. Higgins, *Joule* **2023**, *7*, 1415–1436, https://doi.org/10.1016/j.joule.2023.06.007.
[38] H. Yang, Y.u Qiao, Z. Chang, H. Deng, X. Zhu, R. Zhu, Z. Xiong, P. He, H. Zhou, *Adv. Mater.* **2021**, *33*, 2102415, https://doi.org/10.1002/adma.202102415.
[39] J. Zhou, L. Zhang, M. Peng, X. Zhou, Y. Cao, J. Liu, X. Shen, C. Yan, T. Qian, *Adv. Mater.* **2022**, *34*, 2200131, https://doi.org/10.1002/adma.202200131.
[40] Haoyu Li, Yu Ren, Yue Zhu, Jiaming Tian, Xinyi Sun, Chuanchao Sheng, Ping He, Shaohua Guo, Haoshen Zhou, *Angew. Chem. Int. Ed.* **2023**, *62*, https://doi.org/10.1002/anie.202310143.
[41] L. Wang, B. Zhang, W. Zhou, Z. Zhao, X. Liu, R. Zhao, Z. Sun, H. Li, X. Wang, T. Zhang, H. Jin, W. Li, A. Elzatahry, Y. Hassan,

H. J. Fan, D. Zhao, D. Chao, *J. Am. Chem. Soc.* **2024**, *146*, 6199–6208, https://doi.org/10.1021/jacs.3c14019.
[42] X. Liang, J. Hao, B. Tan, X. Lu, W. Li, *J. Power Sources* **2020**, *472*, 228507, https://doi.org/10.1016/j.jpowsour.2020.228507.
[43] F. Gong, Y. Feng, Y.-H. Fang, Y.-K. Hsu, Y.-C. Chen, *ACS Appl. Mater. Interfaces* **2023**, *15*, 18808–18818, https://doi.org/10.1021/acsami.2c22728.
[44] B. Fei, Z. Liu, J. Fu, X. Guo, K.e Li, C. Zhang, X. Yang, D. Cai, J.i Liu, H. Zhan, *Adv. Funct. Mater.* **2023**, *33*, 2215170, https://doi.org/10.1002/adfm.202215170.
[45] Y. Ran, J. Ren, Z. C. Yang, H. Zhao, Y. Wang, Y. Lei, *Small Struct.* **2023**, *4*, 2300136, https://doi.org/10.1002/sstr.202300136.
[46] Z. Yao, W. Zhang, X. Ren, Y. Yin, Y. Zhao, Z. Ren, Y. Sun, Q.i Lei, J. Wang, L. Wang, T.e Ji, P. Huai, W. Wen, X. Li, D. Zhu, R. Tai, *ACS Nano* **2022**, *16*, 12095–12106, https://doi.org/10.1021/acsnano.2c02330.
[47] D. Han, S. Wu, S. Zhang, Y. Deng, C. Cui, L. Zhang, Y. Long, H. Li, Y. Tao, Z. Weng, Q.-H. Yang, F. Kang, *Small*, **2020**, *16*, 2001736, https://doi.org/10.1002/smll.202001736.

Manuscript received: October 14, 2025
Revised manuscript received: October 23, 2025
Manuscript accepted: October 23, 2025
Version of record online: November 04, 2025